

# Magnetoconvection and dynamo coefficients III: $\alpha$ -effect and magnetic pumping in the rapid rotation regime

P. J. Käpylä<sup>1,2</sup>, M. J. Korpi<sup>3</sup>, M. Ossendrijver<sup>2</sup>, and M. Stix<sup>2</sup>

<sup>1</sup> Astronomy Division, Department of Physical Sciences, PO BOX 3000, FI-90014 University of Oulu, Finland

<sup>2</sup> Kiepenheuer–Institut für Sonnenphysik, Schöneckstrasse 6, D–79104 Freiburg, Germany

<sup>3</sup> Observatory, PO BOX 14, FI-00014 University of Helsinki, Finland

Received 6 February 2006 / Accepted 2 May 2006

## ABSTRACT

*Aims.* The  $\alpha$ - and  $\gamma$ -effects, which are responsible for the generation and turbulent pumping of large scale magnetic fields, respectively, due to passive advection by convection are determined in the rapid rotation regime corresponding to the deep layers of the solar convection zone.

*Methods.* A 3D rectangular local model is used for solving the full set of MHD equations in order to compute the electromotive force (emf),  $\mathcal{E} = \mathbf{u} \times \mathbf{b}$ , generated by the interaction of imposed weak gradient-free magnetic fields and turbulent convection with varying rotational influence and latitude. By expanding the emf in terms of the mean magnetic field,  $\mathcal{E}_i = a_{ij} \bar{B}_j$ , all nine components of  $a_{ij}$  are computed. The diagonal elements of  $a_{ij}$  describe the  $\alpha$ -effect, whereas the off-diagonals represent magnetic pumping. The latter is essentially the advection of magnetic fields by means other than the underlying large-scale velocity field. Comparisons are made to analytical expressions of the coefficients derived under the first-order smoothing approximation (FOSA).

*Results.* In the rapid rotation regime the latitudinal dependence of the  $\alpha$ -components responsible for the generation of the azimuthal and radial fields does not exhibit a peak at the poles, as is the case for slow rotation, but at a latitude of about  $30^\circ$ . The magnetic pumping is predominantly radially down- and latitudinally equatorward as in earlier studies. The numerical results compare surprisingly well with analytical expressions derived under first-order smoothing, although the present calculations are expected to lie near the limits of the validity range of FOSA.

**Key words.** Convection – MHD – Turbulence – Sun: magnetic fields – Stars: magnetic fields

## 1. Introduction

According to dynamo theory small-scale helical turbulence caused by the convective instability in combination with global rotation, uniform or differential, is the source of the large-scale magnetic structures seen in the Sun and in various other late-type stars (e.g. Parker 1955; Moffatt 1978; Krause & Rädler 1980). The small scales enter the evolution equation of the mean magnetic field via the turbulent electromotive force  $\mathcal{E} = \mathbf{u} \times \mathbf{b}$ . If the mean magnetic field  $\bar{\mathbf{B}}$  varies slowly in time and space, the emf can be represented in terms of  $\bar{\mathbf{B}}$  and its gradients

$$\mathcal{E}_i = a_{ij} \bar{B}_j + b_{ijk} \frac{\partial \bar{B}_j}{\partial x_k} + \dots, \quad (1)$$

where  $a_{ij}$  and  $b_{ijk}$  are in the general case tensors containing the transport coefficients, and the dots indicate that higher order derivatives can be taken into account. The challenge is to derive the tensors  $a_{ij}$  and  $b_{ijk}$  which, in general, cannot be done from first principles due to the lack of a comprehensive theory of convective turbulence.

In the kinematic regime where the magnetic energy is negligible in comparison to the kinetic energy the most simple approximation is to neglect all correlations higher than second order in the fluctuations. This is often called the first order smoothing (FOSA), quasilinear, or the second order correlation approximation (SOCA). Considering the simple case of isotropic turbulence in the high-conductivity limit as an example where the transport coefficients can be computed analytically, the tensor  $a_{ij}$  reduces into a single scalar (Steenbeck & Krause 1969)

$$\alpha = -\frac{1}{3} \tau_c \overline{\boldsymbol{\omega} \cdot \mathbf{u}}, \quad (2)$$

where  $\tau_c$  is the correlation time of the turbulence,  $\boldsymbol{\omega} = \nabla \times \mathbf{u}$  the vorticity, and  $\boldsymbol{\omega} \cdot \mathbf{u}$  the kinetic helicity. We note that in the anisotropic case the trace of the tensor  $a_{ij}$ , instead of any individual component of the  $\alpha$ -effect, is proportional to the kinetic helicity (e.g. Rädler 1980; see also Sect. 4.4).

Despite the limited applicability of Eq. (2), numerical models of magnetoconvection have shown that there is at least a qualitative agreement between the  $\alpha$ -effect and the negative of the kinetic helicity also in the anisotropic case (Brandenburg et al. 1990; Ossendrijver et al. 2001, hereafter Paper I). Furthermore, using local time-distance helioseismology, Gizon & Duvall (2003) studied the correlation of the curl and divergence of the horizontal components of solar surface flows as a proxy for the helicity (see also Rüdiger et al. 1999) and found that the correlation follows a  $\cos\theta$  latitude profile for the observed latitude range. Using local numerical convection models Egorov et al. (2004) were able to reproduce the  $\cos\theta$  latitude profile and further confirmed the validity of the correlation as a valid tracer of the helicity. In a recent study, Käpylä et al. (2004) found a similar latitude dependence for moderate rotation, i.e. up to Coriolis number  $\text{Co} = 2\Omega l/u < 4$ , in agreement with the results of Egorov et al. For more rapid rotation,  $\text{Co} \approx 10$ , however, the same authors found that the latitude distribution of the volume average over the convectively unstable region resembles more a  $\sin\theta$  profile for latitudes higher than  $15^\circ$ . As our working hypothesis, we consider the relation (2) to trace the  $\alpha$ -effect, which raises the question of the latitude dependence of this effect in the rapid rotation regime.

In the present study we examine the  $\alpha$ -effect by means of local numerical modelling of small volumes of a star at different latitudes. In distinction to other studies (e.g. Brandenburg et al. 1990; Ossendrijver et al. 2001, 2002, hereafter Paper II), we extend the parameter range in the rapid rotation regime to values typical for the base of the solar convection zone, where the Coriolis number is of the order of 10 or larger (see e.g. Küker et al. 1993; Käpylä et al. 2005b).

As a secondary objective we make an attempt to test the validity of FOSA. A sufficient, but not a necessary, requirement for the applicability of FOSA is that either the Reynolds or the Strouhal number is small

$$\min\left(\frac{ul}{\eta}, uk_f\tau_c\right) = \min(\text{Rm}, \text{St}) \ll 1, \quad (3)$$

where  $u$  and  $l$  are the typical velocity and length scales,  $k_f$  the wavenumber of the energy carrying scale which is related with the correlation length via  $l_c = 2\pi/k_f$ . In the high-conductivity limit relevant for Eq. (2), where  $\eta\tau_c/l_c^2 \ll 1$ , the requirement (3) reduces simply to  $\text{St} \ll 1$  which, however, is at best marginally satisfied (e.g. Brandenburg et al. 2004; Brandenburg & Subramanian 2005b; Käpylä et al. 2006).

We derive analytical formulae for all of the  $a_{ij}$ -coefficients in the high-conductivity limit. For the different components of the  $\alpha$ -effect we find expressions analogous

to Eq. (2) in the anisotropic case. We then compare the analytical result and its numerical equivalent using the correlation time as a free parameter. The correlation time allows us, at least in principle, to compute the Strouhal number.

The remainder of the paper is organised as follows: in Sect. 2 the numerical convection model is described. In Sect. 3 the problem and research methods are stated. In Sects. 4 and 5 we give the results and conclusions, respectively.

## 2. The convection model

### 2.1. Basic equations

The convection model is the same as that presented in Käpylä et al. (2004, 2005b). The computational domain is a rectangular box at latitude  $\Theta$  in the southern hemisphere of a star. The coordinate system of the model is chosen such that  $x$ ,  $y$ , and  $z$  correspond to  $(-\theta, \phi, -r)$  in spherical coordinates, where  $\theta = 90^\circ - \Theta$  is the colatitude. The angular velocity as a function of latitude is given by  $\boldsymbol{\Omega} = \Omega(\cos\Theta\hat{\mathbf{e}}_x - \sin\Theta\hat{\mathbf{e}}_z)$ . The box has horizontal dimensions  $L_x = L_y = 4$ , and  $L_z = 2$  in the vertical direction in units of the depth of the convectively unstable layer  $d$ . We set  $(z_0, z_1, z_2, z_3) = (-0.15, 0, 1, 1.85)$ , where  $z_0$  and  $z_3$  correspond to the top and bottom boundaries of the box, respectively, whereas  $z_1$  and  $z_2$  give the positions of the upper and lower boundaries of the convectively unstable layer. We solve a system of MHD-equations

$$\frac{\partial \mathbf{A}}{\partial t} = \mathbf{u} \times \mathbf{B} - \eta\mu_0\mathbf{J}, \quad (4)$$

$$\frac{\partial \ln \rho}{\partial t} = -(\mathbf{u} \cdot \nabla) \ln \rho + \nabla \cdot \mathbf{u}, \quad (5)$$

$$\begin{aligned} \frac{\partial \mathbf{u}}{\partial t} = & -(\mathbf{u} \cdot \nabla)\mathbf{u} - \frac{1}{\rho}\nabla p - 2\boldsymbol{\Omega} \times \mathbf{u} + \mathbf{g} + \\ & + \frac{1}{\rho}\mathbf{J} \times \mathbf{B} + \frac{1}{\rho}\nabla \cdot (2\nu\rho\mathbf{S}), \end{aligned} \quad (6)$$

$$\begin{aligned} \frac{\partial e}{\partial t} = & -(\mathbf{u} \cdot \nabla)e - \frac{p}{\rho}(\nabla \cdot \mathbf{u}) + \frac{\eta\mu_0}{\rho}\mathbf{J}^2 + \\ & + \Gamma_{\text{cond}} + \Gamma_{\text{visc}} - \Gamma_{\text{cool}}, \end{aligned} \quad (7)$$

where  $\mathbf{A}$  is the magnetic vector potential,  $\mathbf{u}$  the velocity,  $\mathbf{B} = \nabla \times \mathbf{A} + \mathbf{B}_0$  the magnetic field which is the sum of the fluctuating and (constant) imposed contributions,  $\mathbf{J} = \nabla \times \mathbf{B}/\mu_0$  the current density,  $\rho$  the mass density,  $p$  the pressure,  $\mathbf{g} = g\hat{\mathbf{e}}_z$  the constant gravity,  $\hat{\mathbf{e}}_z$  the unit vector in the vertical direction,  $\mathbf{S}_{ij} = \frac{1}{2}(u_{i,j} + u_{j,i} - \frac{2}{3}\delta_{ij}\nabla \cdot \mathbf{u})$  the strain tensor, and  $e = c_V T$  the internal energy per unit mass.  $\mu_0$  is the vacuum permeability,  $\eta$  and  $\nu$  the constant magnetic diffusivity and kinematic viscosity.  $\Gamma_{\text{cond}}$  describes thermal conduction (see the next subsection). The term  $\Gamma_{\text{visc}}$  describes viscous heating via

$$\Gamma_{\text{visc}} = 2\nu\mathbf{S}_{ij}\frac{\partial u_i}{\partial x_j}. \quad (8)$$

The uppermost layer of the box is cooled according to

$$\Gamma_{\text{cool}} = \frac{1}{t_{\text{cool}}} f(z)(e - e_0), \quad (9)$$

where  $t_{\text{cool}}$  is a cooling time, chosen to be so short that the upper boundary stays isothermal,  $f(z) = (z - z_1)/(z_0 - z_1)$  a function which is applied in the interval  $z_0 \leq z < z_1$ , and  $e_0 = e(z_0)$  the value of internal energy (temperature) at the top of the box. The cooling term serves as a parametrisation of the radiative losses occurring at the surface of the star. We assume an ideal gas with

$$p = \rho e(\gamma - 1), \quad (10)$$

where the ratio of the specific heats  $\gamma = c_P/c_V = 5/3$ .  $e_0$  and the stratification in the box are fixed by the parameter

$$\xi_0 = \frac{(\gamma - 1)e_0}{gd}, \quad (11)$$

which defines the pressure scale height at the top of the box.

## 2.2. Boundary conditions and initial setup

We adopt periodic boundary conditions in the horizontal directions, and closed stress free boundaries at the top and at the bottom

$$\frac{\partial u_x}{\partial z} = \frac{\partial u_y}{\partial z} = u_z = 0 \quad \text{at } z = z_0, z_3. \quad (12)$$

For the vector potential we use

$$\frac{\partial A_x}{\partial z} = \frac{\partial A_y}{\partial z} = A_z = 0 \quad \text{at } z = z_0, z_3, \quad (13)$$

which constrain the fluctuating magnetic field to be vertical at the boundaries. We split the heat conduction term into two parts

$$\Gamma_{\text{cond}} = \nabla \cdot [\kappa_t \nabla(e - \bar{e}) + \kappa_h \nabla \bar{e}], \quad (14)$$

where the first term acts only on the fluctuations and the latter only on the mean, i.e. horizontally averaged, stratification. Thus  $\kappa_t$  and  $\kappa_h$  can be considered as the turbulent and radiative conductivities, which satisfy  $\kappa_t \gg \kappa_h$  in real stars. We define the conductivities as

$$\kappa_t = \gamma \rho \chi_0, \quad (15)$$

$$\kappa_h = \frac{(\gamma - 1)F_r}{g\nabla}, \quad (16)$$

where  $\chi_0$  is the reference value of the thermal diffusivity,  $F_r$  the input energy flux, and  $\nabla$  the mean logarithmic temperature gradient in the initial state.

As a boundary condition we fix the temperature at the top of the box and apply a constant mean temperature gradient at the bottom

$$e_{z=z_0} = e_0, \quad (17)$$

$$\frac{\partial e}{\partial z}_{z=z_3} = \frac{g}{(\gamma - 1)} \nabla_3, \quad (18)$$

where  $\nabla_3$  is the logarithmic temperature gradient at the lower boundary (see below).

Initially the radiative flux,  $F_{\text{rad}} = \kappa_h \nabla \bar{e}$ , carries the whole energy through the domain. In the present paper the uppermost layer is initially isothermal, and the stratification in the convectively unstable region is described by a polytropic index  $m_2$ . Often  $m_2 = 1$  is chosen, but this has the disadvantage that the time needed to reach the final thermally relaxed state which is much closer to the adiabatic stratification becomes large (of the order of  $t_{\text{relax}} = \rho \gamma d^2 / \kappa_h \approx 4 \cdot 10^3 \sqrt{d/g}$  in the present study, see also Brandenburg et al. 2005). Thus in practice, only the conductivity  $\kappa_h$  strictly corresponds to the case  $m_2 = 1$  in the initial state, but the thermal stratification corresponds to polytropic index  $m_2 = 1.25$  which is already close to the thermally saturated state. The initial temperature gradient in the lower part of the convectively unstable layer and the overshoot layer is calculated from

$$\nabla(z) = \nabla_3 + \frac{1}{2} \{ \tanh[4(z_m - z)] + 1 \} \Delta \nabla, \quad (19)$$

where  $\nabla_3$  is the imposed gradient, and  $\Delta \nabla = \nabla_2 - \nabla_3$  the difference between the temperature gradients in the convectively unstable layer and the bottom boundary.  $z_m$  is calculated on the condition that  $\nabla = \nabla_{\text{ad}} = (\gamma - 1)/\gamma$  at  $z = z_2$  in the initial non-convecting state. The density stratification is obtained via the equation of hydrostatic equilibrium.

Furthermore, we decrease the input energy flux by a factor of roughly ten in comparison to Papers I and II. Decreasing  $F_r$  even further would be desirable, given the fact that the ratio of the input flux in the model to the solar energy flux is still  $F_r/F_\odot \approx 10^7$ . However, from Eq. (16) it is seen that  $F_r \propto \kappa_h$  which leads to  $t_{\text{relax}} \propto F_r^{-1}$ . Thus  $F_r$  cannot be decreased by a very large amount without a prohibitively large increase in the needed computational time. We consider the present setup to be a good compromise between real stellar conditions and the computational resources required.

## 2.3. Dimensionless quantities

We measure length with respect to the depth of the unstable layer,  $d = z_2 - z_1$ , density in units of the initial value at the bottom of the convectively unstable layer,  $\rho_0$ , and acceleration in units of the gravitational acceleration  $g$ . Furthermore, magnetic permeability is measured in units of  $\mu_0$  and entropy in terms of  $c_P$ . From these choices it follows that time is measured in units of the free fall time,  $\sqrt{d/g}$ , velocity in units of  $\sqrt{dg}$ , magnetic field in terms of  $\sqrt{d\rho_0\mu_0g}$ , and temperature in terms of  $gd/c_P$ .

The calculations are controlled by the following dimensionless parameters. The relative strengths of the thermal and magnetic diffusion against kinetic diffusion are measured by the kinetic and magnetic Prandtl numbers

$$\text{Pr} = \frac{\chi_0}{\nu}, \quad (20)$$

$$\text{Pm} = \frac{\eta}{\nu}, \quad (21)$$

where  $\chi_0$  is the reference value of the thermal diffusivity taken from the middle of the unstably stratified layer.

Rotation is measured by the Taylor number

$$\text{Ta} = \left( \frac{2\Omega d^2}{\nu} \right)^2. \quad (22)$$

A related dimensionless quantity is the Coriolis number, which is the inverse of the Rossby number,  $\text{Co} = 2\Omega\tau$ , where  $\tau = d/u_{\text{rms}}$  is an estimate of the convective turnover time realised in the calculation.

Convection efficiency is measured by the Rayleigh number

$$\text{Ra} = \frac{d^4 g \delta}{\chi_0 \nu H_{\text{ph}}}, \quad (23)$$

where  $\delta = \nabla - \nabla_a$  is the superadiabaticity, measured as the difference between the radiative and the adiabatic logarithmic temperature gradients, and  $H_{\text{ph}}$  is the pressure scale height, both evaluated from the non-convecting initial state in the middle of the unstably stratified layer.

The strength of the imposed magnetic field is described by the Chandrasekhar number

$$\text{Ch} = \frac{\mu_0 B_0^2 d^2}{4\pi \rho_0 \nu \eta}, \quad (24)$$

where  $B_0$  is the magnitude of the imposed field.

We measure the strengths of the advection terms versus the corresponding diffusion terms in the momentum and induction equations by the Reynolds numbers

$$\text{Re} = \frac{u_{\text{rms}} d}{\nu}, \quad (25)$$

$$\text{Rm} = \frac{u_{\text{rms}} d}{\eta}, \quad (26)$$

where  $u_{\text{rms}}$  is the rms value of the velocity fluctuations in the convectively unstable layer. The parameters Pr, Pm, Ta, Ra, and Ch are used as inputs to the model, whereas Re, Rm, and Co are values computed from the actual runs.

The numerical method used is a modified version of that presented in Caunt & Korpi (2001), employing sixth-order accurate explicit finite differences and a third-order accurate Adams-Bashforth-Moulton time stepping routine. The code is parallelised using message passing interface (MPI). The calculations were carried out on the 34-processor BAGDAD Linux cluster hosted by the Kiepenheuer-Institut für Sonnenphysik.

### 3. The $a_{ij}$ -tensor and methods of analysis

#### 3.1. The $a_{ij}$ -tensor

In the present study we concentrate only on the first term of the expansion (Eq. 1)

$$\mathcal{E}_i = a_{ij} \bar{B}_j, \quad (27)$$

which, in the present Cartesian geometry, can be written in matrix form

$$\mathcal{E} = \begin{pmatrix} a_{xx} & a_{xy} & a_{xz} \\ a_{yx} & a_{yy} & a_{yz} \\ a_{zx} & a_{zy} & a_{zz} \end{pmatrix} \begin{pmatrix} \bar{B}_x(z) \\ \bar{B}_y(z) \\ \bar{B}_z \end{pmatrix}, \quad (28)$$

**Table 1.** Summary of the calculations. The following parameters are common for all runs:  $\nu = \eta = 2 \cdot 10^{-4} \sqrt{gd^3}$ ,  $F_r = 3 \cdot 10^{-4} \rho_0 (gd)^{3/2}$ ,  $\nabla_3 = 0.375$ ,  $\xi_0 = 0.2$ ,  $B_0 = 10^{-4} \sqrt{d \rho_0 \mu_0 g}$ , Pr = 0.4, Pm = 1,  $\delta \approx 0.0432$ , and  $H_{\text{ph}} \approx 0.422d$ . These choices result in Ch = 0.02 and  $\text{Ra} \approx 1.03 \cdot 10^6$ . A grid of  $128^3$  is used. The quantities Re, Rm, Co and  $u_{\text{rms}}$  are averages over the convective layer and time, whereas Ta and  $\Theta$  are fixed. We estimate that  $\eta\tau_c/l_c^2 \approx 10^{-3}$  in all of the calculations, see Sect. 4.4.

Run	Re, Rm	Ta	Co	$u_{\text{rms}}$	$\Theta$
Co1-90	257	$6.5 \cdot 10^4$	1.02	0.051	$-90^\circ$
Co1-60	260	$6.5 \cdot 10^4$	1.00	0.052	$-60^\circ$
Co1-30	264	$6.5 \cdot 10^4$	0.99	0.053	$-30^\circ$
Co1-00	253	$6.5 \cdot 10^4$	1.02	0.051	$0^\circ$
Co4-90	241	$1.0 \cdot 10^6$	4.40	0.048	$-90^\circ$
Co4-60	247	$1.0 \cdot 10^6$	4.38	0.049	$-60^\circ$
Co4-30	267	$1.0 \cdot 10^6$	4.00	0.054	$-30^\circ$
Co4-00	319	$1.0 \cdot 10^6$	3.30	0.064	$0^\circ$
Co10-90	209	$6.5 \cdot 10^6$	13.2	0.042	$-90^\circ$
Co10-75	211	$6.5 \cdot 10^6$	13.0	0.042	$-75^\circ$
Co10-60	213	$6.5 \cdot 10^6$	12.8	0.043	$-60^\circ$
Co10-45	222	$6.5 \cdot 10^6$	12.3	0.044	$-45^\circ$
Co10-30	250	$6.5 \cdot 10^6$	10.7	0.050	$-30^\circ$
Co10-15	283	$6.5 \cdot 10^6$	9.38	0.057	$-15^\circ$
Co10-00	408	$6.5 \cdot 10^6$	7.23	0.082	$0^\circ$

where we note that the horizontal mean magnetic fields can vary as function of depth due to the contributions generated by the fluid motions in the course of the calculation. It suffices to make three calculations with uniform magnetic fields imposed along each coordinate axis to obtain all nine components of the  $a_{ij}$ -tensor. This is done separately for each rotation rate and latitude.

Separating the symmetric and antisymmetric parts of the tensor one arrives at (see e.g. Rädler 1980)

$$\alpha_{ij} = (a_{ij} + a_{ji})/2, \quad (29)$$

$$\gamma_i = -\varepsilon_{ijk} a_{jk}/2, \quad (30)$$

where  $\alpha_{ij}$  is a symmetric tensor whose diagonal components describe the generation of the mean magnetic field and the off-diagonals contribute to the pumping effect.  $\gamma_i$  encompasses the antisymmetric contribution and describes the part of the pumping effect analogous to the advection term in the induction equation. More explicitly, the electromotive force can now be written as

$$\mathcal{E} = \alpha \bar{\mathbf{B}} + \boldsymbol{\gamma} \times \bar{\mathbf{B}}, \quad (31)$$

where  $\alpha$  is a symmetric tensor of second rank and  $\boldsymbol{\gamma}$  the vector defined in Eq. (30). The impact of the off-diagonal components of  $\alpha$  on the pumping effect can most easily be seen by writing (Paper II)

$$\mathcal{E} = \alpha^D \cdot \bar{\mathbf{B}} + \boldsymbol{\gamma}^{(x)} \times \bar{\mathbf{B}}_x + \boldsymbol{\gamma}^{(y)} \times \bar{\mathbf{B}}_y + \boldsymbol{\gamma}^{(z)} \times \bar{\mathbf{B}}_z, \quad (32)$$

where  $\overline{\mathbf{B}}_i = \hat{\mathbf{e}}_i \overline{B}_i$ , and

$$\boldsymbol{\alpha}^D = \begin{pmatrix} \alpha_{xx} \\ \alpha_{yy} \\ \alpha_{zz} \end{pmatrix}, \quad (33)$$

$$\boldsymbol{\gamma}^{(x)} = \boldsymbol{\gamma} + \begin{pmatrix} 0 \\ -\alpha_{xz} \\ \alpha_{xy} \end{pmatrix}, \quad (34)$$

$$\boldsymbol{\gamma}^{(y)} = \boldsymbol{\gamma} + \begin{pmatrix} \alpha_{yz} \\ 0 \\ -\alpha_{xy} \end{pmatrix}, \quad (35)$$

$$\boldsymbol{\gamma}^{(z)} = \boldsymbol{\gamma} + \begin{pmatrix} -\alpha_{yz} \\ \alpha_{xz} \\ 0 \end{pmatrix}. \quad (36)$$

Eqs. (34) to (36) show that the pumping velocity can be different for different magnetic field components (Kichatinov 1991, Paper II). Note that in contrast to Eq. (31), which is independent of the chosen coordinate system, the coefficients  $\boldsymbol{\alpha}^D$  and  $\boldsymbol{\gamma}^{(i)}$  in the coordinate dependent Eq. (32) are not vectors on account of their transformation properties.

In what follows, we refer to the  $\alpha$ -effect as the diagonal part of  $a_{ij}$  defined through Eq. (33), in distinction to many earlier studies where it is considered as the full  $\boldsymbol{\alpha}\overline{\mathbf{B}}$  contribution to Eq. (31) (e.g. Krause & Rädler 1980; Rädler 1980; Rädler & Stepanov 2006a). Furthermore,  $\boldsymbol{\gamma}$ , defined as the off-diagonal part of  $a_{ij}$  via Eq. (30), is from now on referred to as the general pumping effect, whereas the  $\boldsymbol{\gamma}^{(i)}$ , defined via Eqs. (34)-(36), describe the field-direction dependent pumping effect.

### 3.2. Summary of the computations and averaging techniques

Table 1 summarises the calculations. A parent run was evolved without rotation or magnetic fields until convection achieved a statistically steady state. In the present case the length of the parent run is  $t = 100$  in units of  $\sqrt{d/g}$ . The final state of this run was used as an initial condition for the runs in Table 1 for which an appropriate rotation vector was imposed. These purely hydrodynamical runs were evolved up to  $t_0 = 500\sqrt{d/g}$  in order to minimize the effects of the transients due to the added rotation and to allow time for thermal relaxation. After this an uniform magnetic field was added.

Similarly as in Paper II we reset the fluctuating component of the magnetic field after every  $T = 50\sqrt{d/g}$  time units in order to minimize the contamination caused by the generated gradients of mean fields. The resetting interval is two times longer than in Paper II, which is justified by the fact that convection, i.e. the average rms velocities, in the present calculations are slower by approximately the same factor (see Table 1) due to the smaller input energy flux  $F_r$ . In the averaging, the first  $\Delta t_f = 10\sqrt{d/g}$  and the last  $\Delta t_l = 30\sqrt{d/g}$  time units of each subinterval are neglected in accordance with the procedure of Paper

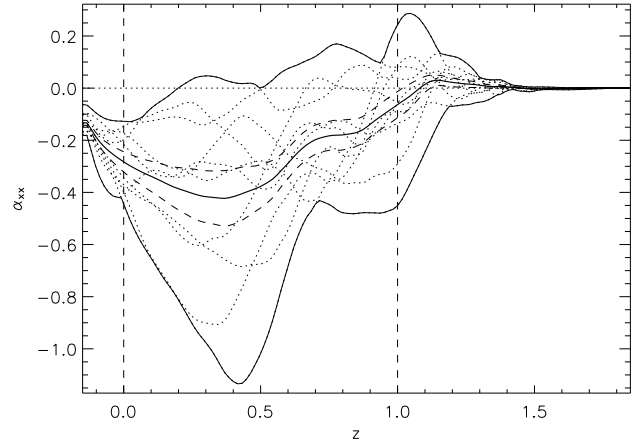


**Fig. 1.** Variation of  $\alpha_{xx} \approx \mathcal{E}_x/\overline{B}_x(z)$  in units of  $0.01\sqrt{dg}$  in the run Co1-90 with an imposed field in the  $x$ -direction. Note that  $\overline{B}_z(z) = 0$ ,  $\max(|\overline{B}_y(z)|/|\overline{B}_x(z)|) = \mathcal{O}(0.1)$ , and  $\max(|\frac{\partial \overline{B}_x(z)}{\partial z}|/|\overline{B}_x(z)|) = \mathcal{O}(0.1d^{-1})$ , indicating that their influence on  $\alpha_{xx}$  is only minor. The dotted curves show the average values from each of the 10 individual subintervals. The thick solid curve shows the average of the 10 curves, and the dashed lines indicate the error estimates computed from the standard deviation  $\sigma$  of the subaverages according to  $\sigma/\sqrt{N}$ . The thin solid lines indicate the full range, denoted from now on by  $\tilde{\sigma}$ , of values attained in the  $N = 10$  subintervals. The vertical dashed lines at  $z = 0$  and  $z = 1$  denote the top and bottom of the convectively unstable region, respectively.

II. The generated mean fields in this subinterval are also taken into account when computing the coefficients  $a_{ij}$ . As demonstrated in Paper II, only a few subintervals are needed for convergence. In the present study the results are averages over 10 subintervals.

The horizontal and time average of a quantity  $f$  over the  $i$ th subinterval is defined via

$$\overline{f}_i(z) = \frac{1}{\Delta t L^2} \int_{-\frac{1}{2}L}^{\frac{1}{2}L} \int_{-\frac{1}{2}L}^{\frac{1}{2}L} \int_{t_0+iT+\Delta t_f}^{t_0+(i+1)T-\Delta t_l} f(x, y, z, t) dx dy dt, \quad (37)$$

where  $L = L_x = L_y$ , and  $\Delta t = T - \Delta t_f - \Delta t_l$  is the length of the subinterval in time. Thus we obtain  $N$  realisations of the quantity  $\overline{f}_i(z)$  that can be considered independent. An additional average over these  $N$  values is simply

$$\overline{f}(z) = \frac{1}{N} \sum_{i=0}^{N-1} \overline{f}_i(z), \quad (38)$$

where  $\overline{f}(z)$  will be the final result. An error estimate can be made by computing the standard deviation  $\sigma$  of the quantity  $\overline{f}(z)$  and dividing it by the square root of the number of the independent realisations, or to show the full range of values attained in the  $N$  subintervals. See Fig. 1 for a typical result.

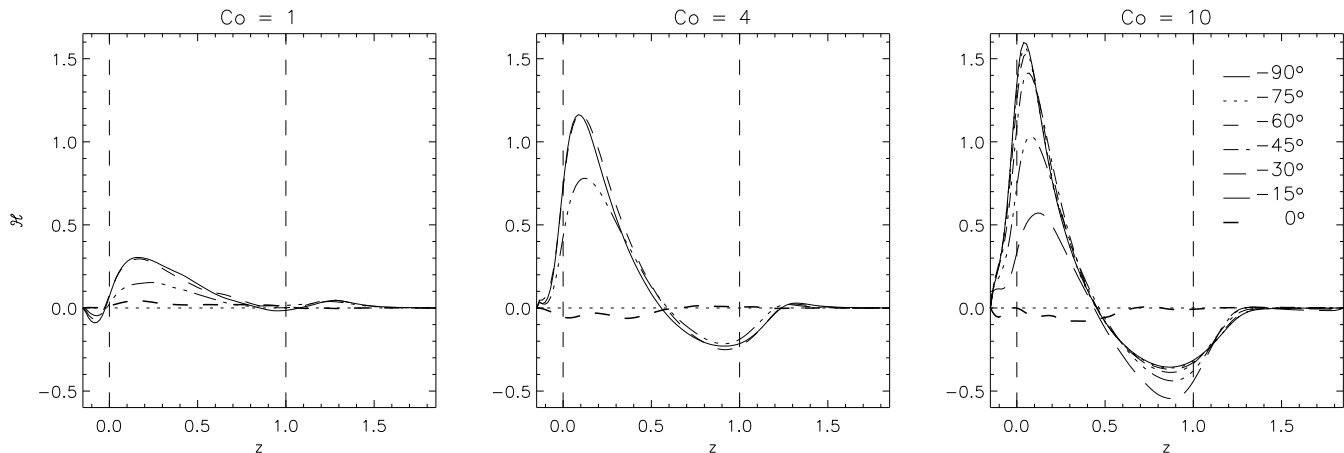


**Fig. 2.** Kinetic helicity  $\mathcal{H} = \overline{\boldsymbol{\omega} \cdot \boldsymbol{u}}$  in units of  $0.01 g$  for the approximate Coriolis numbers 1 (left), 4 (middle), and 10 (right). Each curve corresponds to a different latitude as indicated in the rightmost panel. The top and bottom of the convectively unstable regions are denoted by dashed vertical lines.

## 4. Results

### 4.1. Kinetic helicity

Earlier numerical studies of the  $\alpha$ -effect have shown that the FOSA result, Eq. (2), which states that  $\alpha$  is proportional to the negative of the kinetic helicity holds at least qualitatively (Brandenburg et al. 1990; Paper I). Recent local helioseismic studies have been able to extract information on the kinetic helicity,  $\mathcal{H}$ , in the surface layers of the Sun using the correlation of the horizontal components of the divergence and the curl of the flow as a proxy (Gizon & Duvall 2003). The result is that for the observed latitude range up to the latitude  $\Theta \approx \pm 45^\circ$ , the correlation follows a  $\cos \theta$  latitude profile. Using numerical convection models Egorov et al. (2004) showed that the correlation can indeed be used to map the helicity. These authors were also able to reproduce the observed result with a Coriolis number  $\text{Co} \approx 0.1$  which is consistent with the fact that the observations correspond to the uppermost 20 Mm of the solar surface where the Coriolis number is of this order of magnitude.

However, in a recent study Käpylä et al. (2004) found that the kinetic helicity, averaged over the convectively unstable layer, changes sign as the Coriolis number is increased to the range expected in the deep layers of the solar convection zone,  $\text{Co} \approx 10$ . This result is in apparent contradiction to analytical theory (Rüdiger et al. 1999) and the observational and numerical results mentioned above. This discrepancy, however, turns out to be partly due to the volume averaging performed by Käpylä et al. (2004), although some apparently new features are also present. Fig. 2 shows  $\mathcal{H} = \overline{\boldsymbol{\omega} \cdot \boldsymbol{u}}$  for the present calculations with Coriolis numbers 1, 4, and 10. It is seen that whereas  $\mathcal{H}$  is mostly positive at all depths for  $\text{Co} = 1$ , there is a negative region in the deep layers of the convection zone and the overshoot layer for more rapid rotation. The latitude trend detected by Käpylä et al. (2004) is due to the fact that the region of negative helicity expands

towards the equator whilst the positive peak near the top shrinks. Furthermore, the values near the top seem to follow the more familiar  $\cos \theta$  trend even for  $\text{Co} \approx 10$ . These results suggest that if Eq. (2) holds, the latitudinal behaviour of the  $\alpha$ -effect should mostly change in the deep layers and the overshoot region, but not so much in the upper layers of the convection zone. One must bear in mind, however, that Eq. (2) holds only for the isotropic case, and that anisotropic expressions derived under FOSA give significantly different results and are in better agreement with the numerical results (see Sect. 4.4).

### 4.2. The $\alpha$ -effect

The diagonal components of the  $a_{ij}$  tensor describe the  $\alpha$ -effect which is responsible for the generation of large scale magnetic fields in solar and stellar dynamo models. In other contexts, we note that dynamos can also be supported by the off-diagonal components of  $\boldsymbol{\alpha}$  (e.g. Rädler & Stepanov 2006b) or via the  $\overline{\boldsymbol{\Omega}} \times \overline{\boldsymbol{J}}$  (Rädler 1969, 1986; Roberts 1972) and  $\overline{\boldsymbol{W}} \times \overline{\boldsymbol{J}}$ -effects (Rogachevskii & Kleeorin 2003, 2004) that involve rotation and shear flows in conjunction with large scale gradients of the mean fields, respectively. The present results for  $\alpha_{xx}$ ,  $\alpha_{yy}$ , and  $\alpha_{zz}$  correspond to  $\alpha_{\theta\theta}$ ,  $\alpha_{\phi\phi}$ , and  $\alpha_{rr}$  in spherical coordinates, respectively. Although the present study concentrates on the rapid rotation regime, we have also made calculations with smaller Coriolis numbers in order to facilitate comparison to earlier results. Fig. 3 shows the  $\boldsymbol{\alpha}^D$  components for  $\text{Co} = 1$ . The horizontal components  $\alpha_{xx}$  and  $\alpha_{yy}$  show an expected negative value in the convection zone, but basically zero in the overshoot. Latitudinal behaviour of the horizontal components is consistent with a  $\cos \theta$  profile (see Fig. 6) and is in accordance with the results for the kinetic helicity (Fig. 2).

This is of interest for the solar dynamo, where the poloidal magnetic field is generated from the toroidal one mainly through  $\alpha_{\phi\phi}$ . To lowest order in rotation, this com-

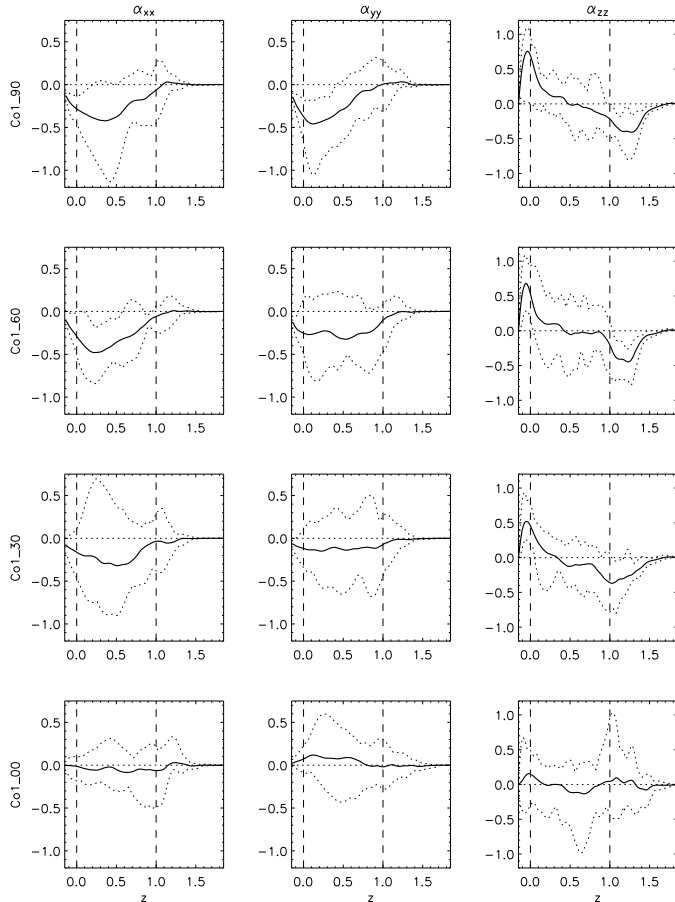


**Fig. 3.** Diagonal components of the  $\alpha$ -tensor in units of  $0.01\sqrt{a}g$  for the Co1 set as functions of depth and in steps of  $\Delta\Theta = 30^\circ$  from the south pole (top) to the equator (bottom). The dashed vertical lines denote the top ( $z = 0$ ) and bottom ( $z = 1$ ) of the convectively unstable region. The dotted curves show the full range of values attained in the 10 subintervals (see Fig. 1).

ponent can be represented by  $\alpha_{\phi\phi} = \alpha_1 \hat{g} \cdot \hat{\Omega} \propto \cos\theta$ , where  $\hat{g}$  and  $\hat{\Omega}$  are the unit vectors of the gradient of turbulence intensity (or equivalently density), and angular velocity, respectively (Krause & Rädler 1980). The sign of the vertical component,  $\alpha_{zz}$ , is opposite to those of the horizontal components (see also Brandenburg et al. 1990; Paper I) and the magnitude of this quantity is comparable to the horizontal components in the convectively unstable zone and clearly larger, and negative, in the overshoot region. The latitude profile is consistent with  $\cos\theta$  in the convection zone and more or less constant in the overshoot layer at least up to  $\Theta = -30^\circ$ .

The results for  $Co = 4$  are very similar to those obtained for  $Co \approx 2.4$  in Paper II, see Fig. 4. Here the noteworthy piece of information is the increased anisotropy of the  $\alpha$ s: whereas for  $Co = 1$  the horizontal components were both consistent with a  $\cos\theta$  latitude profile, for  $Co = 4$  only  $\alpha_{xx}$  follows this trend.  $\alpha_{yy}$ , on the other hand, is basically constant as function of latitude at least up to the latitude  $-30^\circ$ . Furthermore, a region of opposite sign

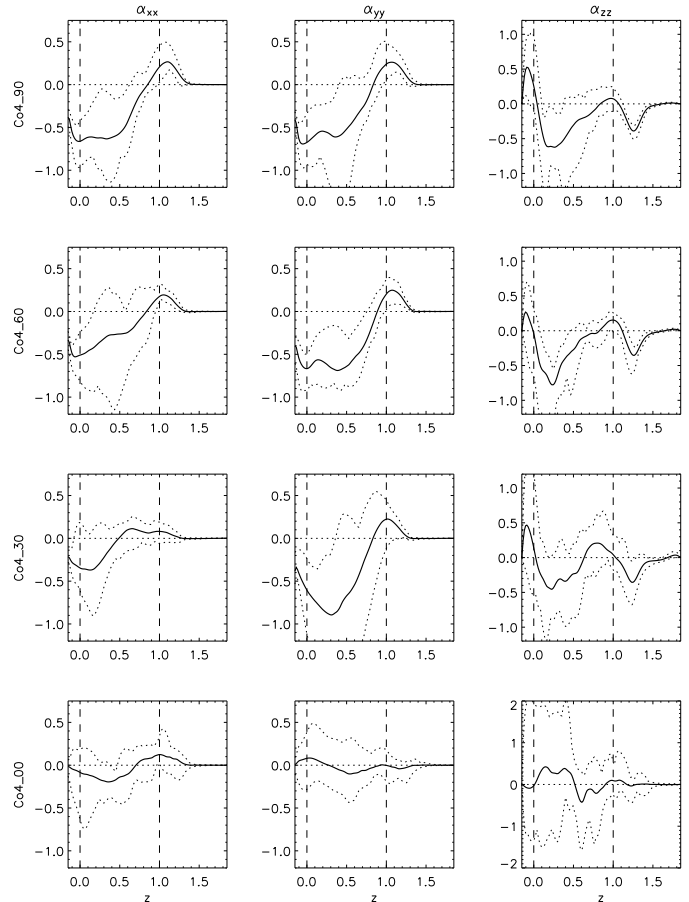


**Fig. 4.** Diagonal components of the  $\alpha$ -tensor for the Co4 set, otherwise the same as Fig. 3.

appears in the overshoot region, consistent with the trend seen in the kinetic helicity (Fig. 2). The vertical component  $\alpha_{zz}$  predominantly shows a mixed sign, but there are indications of a region with negative sign near the top, a trend that will emerge much more strongly for more rapid rotation (see Fig. 5). The latitude trend of  $\alpha_{zz}$  is similar to that of  $\alpha_{yy}$ .

The previous numerical studies of the  $\alpha$ -effect have not gone far beyond  $Co = 1$ , although, using mixing length models as a guide, it can be estimated that the Coriolis number is of the order of 10 or larger in the deep layers of the solar convection zone (Käpylä et al. 2005b). Fig. 5 presents results for rapid rotation, i.e.  $Co = 10$ . There are some distinct differences to the models with slower rotation. First of all,  $\alpha_{xx}$  changes its sign between latitudes  $45^\circ$  and  $60^\circ$  in the convection zone. Note that the figure shows the full range of values from the ten subintervals, and that the actual error is significantly smaller (see Fig. 7). The value in the overshoot layer, however, still peaks at the pole and diminishes monotonically towards the equator, although in a rather steeper fashion than  $\cos\theta$  (see Fig. 7). It is also noteworthy that the magnitude of  $\alpha_{xx}$  in the convection zone becomes small in comparison to that of  $\alpha_{yy}$ .

Perhaps the most interesting change that can be observed in the rapid rotation regime is the strikingly different latitude dependence of  $\alpha_{yy}$  (see Fig. 7); the value in the convection zone now peaks at latitude  $-30^\circ$ , whereas the value in the overshoot is basically constant as function of latitude all the way down to  $\Theta = -15^\circ$ . Furthermore, the sign of the vertical  $\alpha$  is now totally reversed in comparison to the case of  $\text{Co} = 1$ . The maximum values of  $\alpha_{zz}$  in the convection zone and the overshoot layer also occur at intermediate latitudes  $\Theta = -30^\circ \dots -45^\circ$ .

We note that the trend of the horizontal  $\alpha$ -effect as a function of rotation at the pole, where  $\alpha_{xx} = \alpha_{yy}$ , is consistent with the behaviour found in Paper I. Also the sign change of  $\alpha_{zz}$  is reproduced. Analytical theory (Rüdiger & Kichatinov 1993) predicts that the horizontal  $\alpha$ -effect should saturate to a constant value when  $\text{Co}$  is large enough. This seems to occur for  $\alpha_{yy}$  in the convection zone at and near the pole where the values stay more or less constant for all Coriolis numbers. The values in the overshoot layer and in the convection zone at lower latitudes, however, do not seem to show saturation; according to the study of Rüdiger & Kichatinov (1993)  $\alpha_{yy}$  grows roughly 15 per cent when  $\text{Co}$  is increased from 4 to 10, whereas in the present results the increase is significantly more. It cannot be ruled out, however, that signs of saturation could already be seen if calculations with intermediate Coriolis numbers were made or whether saturation occurs when rotation is more rapid than in the present study. The prediction of Rüdiger & Kichatinov (1993) of a vanishing vertical  $\alpha$ -effect for rapid rotation is not realised in the present results.

### 4.3. Magnetic pumping

The existence of field direction dependent pumping of the mean field in magnetoconvection calculations was established in Paper II. We find that the qualitative results of the present study are not significantly different from those obtained in Paper II. The main results for the general pumping effect, Eq. (30), in the rapid rotation case are shown in Fig. 8. The latitudinal pumping effect,  $\gamma_x$ , is positive, i.e. equatorward in the bulk of the convection zone and essentially zero in the overshoot layer. The maximum of  $\gamma_x$  is near the equator,  $\Theta = -15^\circ$ , where the value can be as high as 25 per cent of the turbulent rms-velocity. If we consider the model to describe the deep layers of the solar convection zone where  $u \approx 10 \text{ m s}^{-1}$  according to mixing length models, the latitudinal pumping velocity would correspond to a velocity of  $2.5 \text{ m s}^{-1}$ , which is of the same order of magnitude as the expected values for the equatorward meridional flow in the deep layers (e.g. Rempel 2005). Taking into account the off-diagonal components of the  $\alpha$ -tensor (Fig. 9), it is seen that the equatorward pumping of the toroidal field,  $\gamma_x^{(y)} = \gamma_y + \alpha_{yz}$ , is further enhanced by the positive  $\alpha_{yz}$ . The same term enters the equation for the latitudinal pumping of the vertical field with a negative sign and causes  $\gamma_x^{(z)}$  to be some-

what smaller, but due to the small magnitude of  $\alpha_{yz}$  in comparison to  $\gamma_x$ , the qualitative results do not change. We note that in comparison to Paper II the equatorward trend of the general latitudinal pumping effect  $\gamma_x$  is more pronounced in the rapid rotation regime.

The longitudinal component  $\gamma_y$  is predominantly retrograde in the bulk of the convection zone but often exhibits a thin prograde region near the top boundary. The maximum occurs again rather near the equator at  $\Theta = -15^\circ$ . The latitude and depth distribution of  $\alpha_{xz}$  is virtually identical to  $\gamma_y$  but with different sign. This causes the longitudinal pumping of the latitudinal field,  $\gamma_y^{(x)}$ , to become very small at virtually all latitudes, whereas the vertical field is pumped in the retrograde (prograde) direction in the convectively unstable (overshoot) layer with a velocity comparable to that of latitudinal pumping velocity.

The vertical pumping effect is directed mainly downwards, as has been found in various earlier numerical studies (Nordlund et al. 1992; Brandenburg et al. 1996; Tobias et al. 1998, 2001; Paper II; Ziegler & Rüdiger 2003). As was found in Paper II the vertical pumping is dominated by the diamagnetic effect, which tends to transport the magnetic field from regions of large turbulent intensity, characterised by large rms-value of the fluctuating velocity, towards regions of lower intensity (e.g. Rädler 1968; Krause & Rädler 1980). In the anisotropic case (see Eqs. 47 and 48) the vertical pumping is proportional to  $-\partial_z \overline{u_z^2}$ . There is, however, a much stronger latitude dependence of  $\gamma_z$  than in the more moderate rotation cases studied in Paper II, with even a region of upward pumping in the upper layers of the convection zone at low latitudes  $|\Theta| < 15^\circ$ . The vertical pumping of the latitudinal field,  $\gamma_z^{(x)} = \gamma_x + \alpha_{xy}$ , is almost constant as function of latitude in contrast to the strongly varying general vertical pumping  $\gamma_z$ . The pumping of the azimuthal field,  $\gamma_z^{(y)} = \gamma_x - \alpha_{xy}$ , on the other hand, is directed upward at latitudes  $|\Theta| < 45^\circ$ .

### 4.4. Comparison to FOSA

The exact determination of the transport coefficients, such as  $a_{ij}$  and  $b_{ijk}$ , is the most fundamental difficulty in dynamo theory. The problem is basically to choose a closure method that is both practical and accurate. This problem applies already to Eq. (1), where usually only the two first terms are taken into account. Some indications already exist for the need of higher order derivatives in order to accurately describe the electromotive force; see e.g. the numerical geodynamo experiments of Schinnerer et al. (2005). The second part of the closure problem is connected with the derivation of  $\mathcal{E}$  from first principles. The most widely used approximation is to consider only the induction equation of the small-scale field and neglect all higher than second order fluctuations, which is the first-order smoothing approximation (see below). It is possible to extend this approach to take into account higher order contributions (Nicklaus & Stix 1988) using the method of a cumulative



series expansion (van Kampen 1974a,b). However, in this approach the backreaction of the magnetic field to the flow is neglected or at least implicit. Recently, a new approach has been introduced (Blackman & Field 2002; see also Brandenburg & Subramanian 2005a), where instead of  $\mathcal{E}$  itself, the time derivative  $\dot{\mathcal{E}}$  is computed and the higher order contributions,  $\mathbf{T}$ , are retained via a damping term  $\mathbf{T} = -\mathcal{E}/\tau$ . This approach is often called the ‘minimal tau-approximation’ (hereafter MTA), which leads to expressions closely resembling the FOSA results, but with the important distinction that due to the fact that the equation of motion is also used in the derivation, in addition to the kinetic helicity also the small-scale current helicity enters the equation for  $\alpha$ . Recent numerical studies indicate that the current helicity is indeed important for the  $\alpha$ -effect when the magnetic field is dynamically important (Brandenburg & Subramanian 2005b).

In order to compare the present numerical results directly to the mean-field theory we derive analytical expressions describing the coefficients  $a_{ij}$  using the first-order smoothing approximation (FOSA). Thus we generalise Eq. (2) to the case of anisotropic turbulence. The reason to compare to FOSA is that it is relatively straightforward to apply and that the present calculations are in the kinematic regime where the influence of the magnetic field on the flow is weak and thus the contribution of the current helicity is negligible. Furthermore, this comparison will be useful in evaluating the applicability of the approximation itself in dynamo theory. We start from the equation of the fluctuating magnetic field

$$\dot{\mathbf{b}} = \nabla \times (\overline{\mathbf{U}} \times \mathbf{b} + \mathbf{u} \times \overline{\mathbf{B}} + \mathbf{G} - \eta \nabla \times \mathbf{b}), \quad (39)$$

where

$$\mathbf{G} = \mathbf{u} \times \mathbf{b} - \overline{\mathbf{u} \times \mathbf{b}}. \quad (40)$$

We drop the term proportional to  $\overline{\mathbf{U}}$  for the time being. Furthermore, the diffusion term in Eq. (39) can be neglected since  $\eta\tau_c/l_c^2 \approx 10^{-3}$ , where we have used  $\tau_c = 3\sqrt{d/g}$  and  $l_c = 2\pi/k_f \approx d$  (see below).  $\mathbf{G}$  vanishes under the assumptions of FOSA, so we are left with

$$\dot{b}_i = (\delta_{il}\delta_{jm} - \delta_{im}\delta_{jl})\partial_j(u_l\overline{B}_m). \quad (41)$$

The emf is now calculated from

$$\mathcal{E}_i = \varepsilon_{ijk}u_j b_k, \quad (42)$$

where

$$b_k = \int_{-\infty}^t \dot{b}_k dt. \quad (43)$$

Assuming that the correlation time of the turbulence is short and that the mean magnetic field  $\overline{\mathbf{B}}$  varies slowly, Eq. (43) can be integrated. Following this procedure the  $a_{ij}$  tensor components can be derived. Using the assumption that  $\int_0^\infty \overline{u_k(t)\partial_l u_m(t+t')}dt' = \overline{u_k(t)\partial_l u_m(t)}\tau_c$ , with

$\tau_c$  having no dependence on  $k, l$  or  $m$ , we find

$$a_{xx} = \alpha_{xx} = -\tau_c(\overline{u_z\partial_x u_y} - \overline{u_y\partial_x u_z}) \quad (44)$$

$$a_{yy} = \alpha_{yy} = -\tau_c(\overline{u_x\partial_y u_z} - \overline{u_z\partial_y u_x}) \quad (45)$$

$$a_{zz} = \alpha_{zz} = -\tau_c(\overline{u_y\partial_z u_x} - \overline{u_x\partial_z u_y}) \quad (46)$$

$$a_{xy} = \tau_c(\overline{u_y\partial_y u_z} + \overline{u_z\partial_x u_x} + \overline{u_z\partial_z u_z}) \quad (47)$$

$$a_{yx} = -\tau_c(\overline{u_z\partial_y u_y} + \overline{u_x\partial_x u_z} + \overline{u_z\partial_z u_z}) \quad (48)$$

$$a_{xz} = -\tau_c(\overline{u_y\partial_x u_x} + \overline{u_z\partial_z u_y}) \quad (49)$$

$$a_{zx} = \tau_c(\overline{u_x\partial_x u_y} + \overline{u_y\partial_z u_z}) \quad (50)$$

$$a_{yz} = \tau_c(\overline{u_z\partial_z u_x} + \overline{u_x\partial_y u_y}) \quad (51)$$

$$a_{zy} = -\tau_c(\overline{u_x\partial_z u_z} + \overline{u_y\partial_y u_x}) \quad (52)$$

where  $\tau_c$  is the correlation time. In Eqs. (49) to (52), terms of the form  $\overline{u_k\partial_x u_k}$  and  $\overline{u_k\partial_y u_k}$  have vanished due to the horizontal periodicity. In practice, we use  $\tau_c$  as a free parameter when comparing with the numerical data.

Figs. 10 and 11 show all nine components of the  $a_{ij}$  tensor for the calculations Co1-30 and Co10-30. We use  $\tau_c = 3\sqrt{d/g}$  in all of the plots and neglect the possible  $z$ -dependency of  $\tau_c$ . The FOSA expressions for the diagonal components of  $a_{ij}$  seem to best fit to the full numerical results of the corresponding quantities, although the fits seem to become poorer when rotation is increased. The off-diagonal components  $a_{xy}$  and  $a_{yx}$  are reproduced best in sign and magnitude, whereas the sign, but not usually the magnitude, of  $a_{xz}$ ,  $a_{zx}$ , and  $a_{zy}$  is in most cases correct. For  $a_{yz}$  the correspondence is basically non-existent or in the few successful cases it can be considered coincidental. The magnitudes of the off-diagonal components already show that a universal correlation time that would fit all the data cannot be assigned. We note here that the trace of  $a_{ij}$  is proportional to the the negative of the kinetic helicity, i.e.

$$\delta_{ij}a_{ij} = -\tau_c\overline{\boldsymbol{\omega} \cdot \mathbf{u}}. \quad (53)$$

This relation is compared with numerical results in Fig. 12. The correspondence is rather good so that at least the sign is mostly correct. However, the large peak of the helicity near the surface of the convectively unstable region in the moderately and rapidly rotating cases is not well reproduced by the trace of  $a_{ij}$ . This discrepancy, however, seems to diminish at lower latitudes (see the rightmost panels of Fig. 12).

Although the numerical results differ from the FOSA expressions in details, the correspondence is still remarkably good. Very similar results were found also for higher Reynolds numbers, with  $\text{Rm} \approx 400$  and 580 from preliminary higher resolution calculations. It is surprising that the same correlation time gives a reasonably good fit for the  $\alpha$ -effect for all Coriolis numbers, although increasing  $\text{Co}$  is accompanied by a significantly decreased correlation time of the convective motions (see Käpylä et al. 2006) and a similar decrease is also seen when MTA is applied to the Reynolds stresses (Käpylä et al. 2005a). We can also estimate the Strouhal number from

$$\text{St} = u_{\text{rms}}k_f\tau_c, \quad (54)$$

where  $k_f$  is the wavenumber where kinetic energy spectrums peaks. The exact value of  $k_f$  is difficult to assess accurately since it tends to vary in time and also in depth. However, we note that the power always peaks in rather large scales<sup>1</sup>, i.e.  $k_f = (5 \dots 10) d^{-1}$ , with which we obtain values of  $St$  which are of the order of unity or larger. As in Käpylä et al. (2006) we find that  $u_{\text{rms}}$  decreases and  $k_f$  increases as function of rotation, effectively balancing each other so that  $St$  is more or less constant as function of  $Co$ . The values of the Strouhal number obtained by using the correlation time from the fits to analytic FOSA expressions therefore suggest that higher than second order terms should be important for the dynamo coefficients already in the kinematic regime.

## 5. Conclusions

We use three-dimensional modelling of convection in rectangular boxes at different latitudes and Coriolis numbers to study the  $\alpha$ -effect and turbulent magnetic pumping. The results for the  $\alpha$ -effect at moderate and intermediate rotation can be summarised as follows

- As in previous studies (Papers I and II) we find that the horizontal components  $\alpha_{xx}$  and  $\alpha_{yy}$  are negative in the convection zone on the southern hemisphere and follow a more or less  $\cos\theta$  latitude profile for moderate rotation ( $Co = 1$ ). The latitude trend is in accordance with the similar distribution of the kinetic helicity, which, in the simpler case of isotropic turbulence is proportional to the negative of the (scalar)  $\alpha$ -effect. Values of the horizontal  $\alpha$ s in the overshoot region are consistent with zero.
- For  $Co = 4$  we find that the latitude trend for  $\alpha_{xx}$  remains effectively the same as for  $Co = 1$ , whereas the magnitude of the quantity increases. For the same Coriolis number, the component  $\alpha_{yy}$  is more or less constant as function of latitude at least up to  $\Theta \approx -30^\circ$ . A pronounced region of oppositely signed horizontal  $\alpha$ s appear in the overshoot region with latitude distribution similar to the corresponding quantity in the convection zone.
- The vertical component  $\alpha_{zz}$  is positive in the convection zone and negative in the overshoot for  $Co = 1$  and exhibits more sign changes as a function of depth for  $Co = 4$ .

As noted recently by Käpylä et al. (2004), the qualitative behaviour of kinetic helicity changes significantly when rotation is rapid enough, i.e.  $Co \approx 10$ , raising the question of the  $\alpha$ -effect in this regime. This regime also coincides with the deep layers of the solar convection zone. New results for the rapid rotation regime include (see also Fig. 7).

- The  $\alpha_{xx}$  component shows diminishing magnitude and a sign change in the convection zone near the equator

<sup>1</sup> The smallest possible horizontal wavenumber that fits in the box is  $k = 2\pi/L_x = \pi/2$ .

for  $Co = 10$  and a steeper than  $\cos\theta$  trend in the overshoot.

- In the stellar context the most interesting component is  $\alpha_{yy}$ , corresponding to  $\alpha_{\phi\phi}$  in spherical coordinates. Unlike the earlier studies where rotation is not so strong,  $\alpha_{yy}$  in the convection zone no longer peaks at the poles, but rather much closer to the equator at  $\Theta = -30^\circ$ . The value in the overshoot is virtually constant as function of latitude.
- Another new feature is the sign change of  $\alpha_{zz}$ , which now coincides with the azimuthal component. Also the latitudinal distribution is similar, convection zone and overshoot values peaking around  $\Theta = -30^\circ \dots -45^\circ$ .
- The maximum values of the diagonal components of  $a_{ij}$  are of the order of  $0.2 - 0.3 u_{\text{rms}}$ . Considering the models to describe the deep layers of the solar convection zone where  $u \approx 10 \text{ m s}^{-1}$ , the magnitude of these terms would be of the order of  $2 - 3 \text{ m s}^{-1}$ .

The turbulent pumping effects can be summarised as follows

- The latitudinal pumping is equatorward and peaks near the equator, i.e. around  $\Theta = -15^\circ$ . The magnitude of  $\gamma_x$  is maximally about  $0.2 u_{\text{rms}}$ , which would corresponds to  $2 - 3 \text{ m s}^{-1}$  in the deep layers of the solar convection zone.
- Longitudinal pumping is retrograde in the convection zone and prograde near the upper boundary of the domain. At the equator the prograde region is larger.
- Vertical pumping is predominantly directed downwards and dominated by the diamagnetic effect. Whereas the poloidal field is always pumped downwards, the azimuthal field is pumped upwards at low latitudes,  $|\Theta| < 45^\circ$ .

The present new results are likely to have consequences for mean-field models of the solar dynamo. First of all, a long-standing problem of solar dynamo models is that the radial differential rotation is strongest at high latitudes (e.g. Schou et al. 1998) and the often assumed simple form of the  $\alpha$ -effect, proportional to  $\cos\theta$ , imply that the dynamo is most efficient at the poles, but virtually no sunspots are observed at latitudes higher than  $|\Theta| > 40^\circ$ . The tendency of  $\alpha_{yy}$  to peak at latitudes around  $|\Theta| = 30^\circ$  in the regime where the rotational influence is comparable to the bottom of the solar convection zone is likely to alleviate this problem. The second major problem for solar dynamo models is due to the positive radial gradient of the angular velocity near the equator (e.g. Schou et al. 1998) which, with a positive  $\alpha$ -effect in the northern hemisphere, leads to poleward migration of the activity belts (Parker 1987), in contradiction with observations. The latitudinal pumping will most likely also help in alleviating this problem as well, and it has been noted that downward pumping has a similar effect in mean-field models (Brandenburg et al. 1992). The longitudinal pumping velocity  $\gamma_\phi$  plays no role in axisymmetric dynamo models, although its gradients  $\nabla_r \gamma_\phi$  and  $\nabla_\theta \gamma_\phi$  give rise to terms analogous to those

that appear due to differential rotation. The magnitude of this effect, however, is likely to be small in comparison to that of differential rotation. Longitudinal pumping may be important in more general configurations where, for example, the propagation of non-axisymmetric structures could be explained by this effect. The motivation for this is that in the case of the Sun evidence for relatively short-lived nonaxisymmetric structures exists (of the order of 10 rotations from sunspot statistics by Pelt et al. (2006) up to the length of the sunspot cycle of 11 years from solar flares by Bai 2003), whilst for rapidly rotating late-type stars the concept of active longitudes persisting over several stellar cycles is widely accepted (see e.g. Berdyugina & Tuominen 1998).

In order to investigate the applicability of the first-order smoothing approximation (FOSA) we have derived analytical expressions of the transport coefficients which we compare to the quantities obtained numerically. We find rather good correspondence for the  $\alpha$ -effect in the moderate rotation case ( $Co = 1$ ), whereas the off-diagonal components of  $a_{ij}$  are only in qualitative accordance or fail to reproduce even that. For more rapid rotation the fits are poorer, but still manage to capture the qualitative features correctly. The correlation time, used here as a free parameter to fit the numerical data to the analytical expressions, turns out not to have a universal value. Despite of this, we have used  $\tau_c = 3\sqrt{d/g}$  for the whole parameter range investigated, as it seems to reproduce the  $\alpha$ -effect satisfactorily for all rotation rates investigated. With the correlation times obtained from the fitting procedure we can also estimate the Strouhal number, for which we found values of the order of unity independent of rotation. The lack of dependence on rotation results in directly from the universal correlation time used in the fitting which, however, is not consistent with the correlation time computed directly from the flow (Käpylä et al. 2005a, 2006). At the moment the reason for this behaviour is unclear.

In the present study the  $\alpha$ -quenching (e.g. Cattaneo & Vainshtein 1991; Vainshtein & Cattaneo 1992) issue has not received any attention, but we note that exploration of this issue is further required. A related problem concerns the magnetic helicity fluxes (Kleeorin et al. 2000; Vishniac & Cho 2001) and the effects of boundary conditions (Brandenburg & Sandin 2004) on the efficiency of the  $\alpha$ -effect. Furthermore, to date, the  $b_{ijk}$ -tensor components have not to our knowledge been calculated from numerical models of convection. These points, however, cannot be addressed within the scope of the present study but should be explored in the future.

*Acknowledgements.* PJK acknowledges the financial support from the graduate school for astronomy and space physics of the Finnish academy and the Kiepenheuer-Institut for travel support. Furthermore, the Academy of Finland grant 1112020 is acknowledged. The authors wish to thank the referee (Prof. K.-H. Rädler) for his thorough and critical reading of the manuscript and his numerous comments which helped to clarify and improve the paper significantly.

## References

- Bai, T. 2003, *ApJ*, 585, 1114  
 Berdyugina, S. V. & Tuominen, I. 1998, *A&A*, 336, 25L  
 Blackman, E. G. & Field, B. G. 2002, *PhRvL*, 89, 265007  
 Brandenburg, A., Nordlund, Å., Pulkkinen, P., Stein, R. F. & Tuominen, I. 1990, *A&A*, 232, 277  
 Brandenburg, A., Moss, D. & Tuominen, I. 1992, in *The Solar Cycle*, ed. K. L. Harvey, ASP Conf. Series, Vol. 27, 536  
 Brandenburg, A., Jennings, R. L., Nordlund, Å., et al. 1996, *JFM*, 306, 325  
 Brandenburg, A., Käpylä, P. J. & Mohammed, A. 2004, *Physics of Fluids*, 16, 1020  
 Brandenburg, A. & Sandin, C. 2004, *A&A*, 427, 13  
 Brandenburg, A., Chan, K. L., Nordlund, Å., & Stein, R. F. 2005, *AN*, 326, 681  
 Brandenburg, A. & Subramanian, K. 2005a, *PhR*, 417, 1  
 Brandenburg, A. & Subramanian, K. 2005b, *A&A*, 439, 835  
 Cattaneo, F. & Vainshtein, S. I. 1991, *ApJ*, 376, L21  
 Caunt, S. E. & Korpi, M. J. 2001, *A&A*, 369, 706  
 Egorov, P., Rüdiger, G. & Ziegler, U. 2004, *A&A*, 425, 725  
 Gizon, L. & Duvall, T. I. 2003, *Supergranulation Supports Waves*, in *Local and Global Helioseismology: The Present and Future*, ed. H. Sawaya-Lacoste (Noordwijk: ESA Publications Division), 43  
 Käpylä, P. J., Korpi, M. J. & Tuominen, I. 2004, *A&A*, 422, 793  
 Käpylä, P. J., Korpi, M. J., Ossendrijver, M. & Tuominen, I. 2005a, *AN*, 326, 186  
 Käpylä, P. J., Korpi, M. J., Stix, M. & Tuominen, I. 2005b, *A&A*, 438, 403  
 Käpylä, P. J., Korpi, M. J., Ossendrijver, M. & Tuominen, I. 2006, *A&A*, 448, 433  
 Kichatinov, L. L., 1991, *A&A*, 243, 483  
 Kleeorin, N. I., Moss, D., Rogachevskii, I. & Sokoloff, D. 2000, *A&A*, 361, L5  
 Krause F., Rädler, K.-H. 1980, *Mean-Field Magnetohydrodynamics and Dynamo Theory* (Pergamon Press, Oxford)  
 Küker, M., Rüdiger, G. & Kichatinov, L. L. 1993, *A&A*, 279, L1  
 Moffatt, H. K. 1978, *Magnetic field generation in electrically conducting fluids* (Cambridge University Press, Cambridge)  
 Nicklaus, B. & Stix, M. 1988, *Geophys. Astrophys. Fluid Dynamics*, 43, 149  
 Nordlund, Å, Brandenburg, A., Jennings, R. L., et al. 1992, *ApJ*, 392, 647  
 Ossendrijver, M., Stix, M. & Brandenburg, A. 2001, *A&A*, 376, 726 (Paper I)  
 Ossendrijver, M., Stix, M., Brandenburg, A. & Rüdiger, G. 2002, *A&A*, 394, 735 (Paper II)  
 Parker, E. N. 1955, *ApJ*, 122, 293  
 Parker, E. N. 1987, *SoPh*, 110, 11  
 Pelt, J., Brooke, J., Korpi M. J. & Tuominen, I. (2006), submitted to *A&A*  
 Rädler, K.-H. 1968, *Z. Naturforschung*, 23a, 1851  
 Rädler, K.-H. 1969, *Monatsber. Dtsch. Akad. Wiss. Berlin*, 11, 194  
 Rädler, K.-H. 1980, *AN*, 301, 101  
 Rädler, K.-H. 1986, *AN*, 307, 89  
 Rädler, K.-H., Stepanov, R. 2006a, *PhRvE* in press (physics/0512120)

- Rädler, K.-H., Stepanov, R. 2006b, submitted to GAFD (physics/0603085)
- Rempel, M. 2005, ApJ, 622, 1320
- Roberts, P. H. 1972, Phil Trans. R. Soc. London Se. A, 272, 663
- Rogachevskii, I. & Kleeorin, N. 2003, PhRvE, 68, 036301
- Rogachevskii, I. & Kleeorin, N. 2004, PhRvE, 70, 046310
- Rüdiger, G. & Kichatinov, L. L. 1993, A&A, 269, 581
- Rüdiger, G., Brandenburg, A., Pipin, V. V. 1999, AN, 320, 135
- Schrinner, M., Rädler, K.-H., Schmitt, D., Rheinhardt, M. & Christensen, U. 2005, AN, 326, 245
- Schou, J. S., Antia, H. M., Basu, S., et al. 1998, ApJ, 505, 390
- Steenbeck, M. & Krause, F. 1969, AN, 291, 49
- Tobias, S. M., Brummel, N. H., Clune, Th. L. & Toomre, J. 1998, ApJ, 502, L177
- Tobias, S. M., Brummel, N. H., Clune, Th. L. & Toomre, J. 2001, ApJ, 549, 1183
- Vainshtein, S. I. & Cattaneo, F. 1992, ApJ, 393, 165
- van Kampen, N. G. 1974a, Physica, 74, 215
- van Kampen, N. G. 1974b, Physica, 74, 239
- Vishniac, E. T. & Cho, J. 2001, ApJ, 550, 752
- Ziegler, U. & Rüdiger 2003, A&A, 401, 433

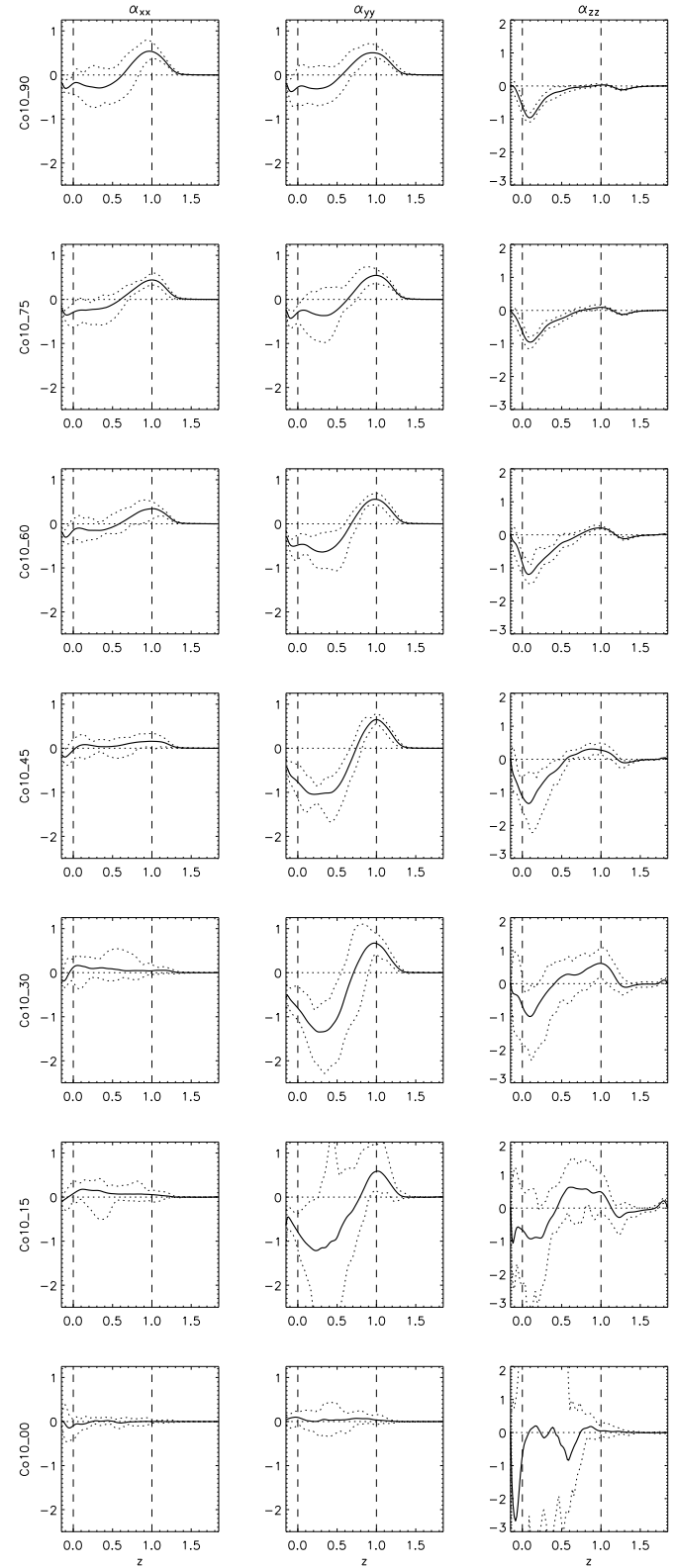


**Fig. 5.** Diagonal components of the  $\alpha$ -tensor for the Co10 set in steps of  $\Delta\Theta = 15^\circ$  from the south pole (top) to the equator (bottom). Otherwise the same as Fig. 3.

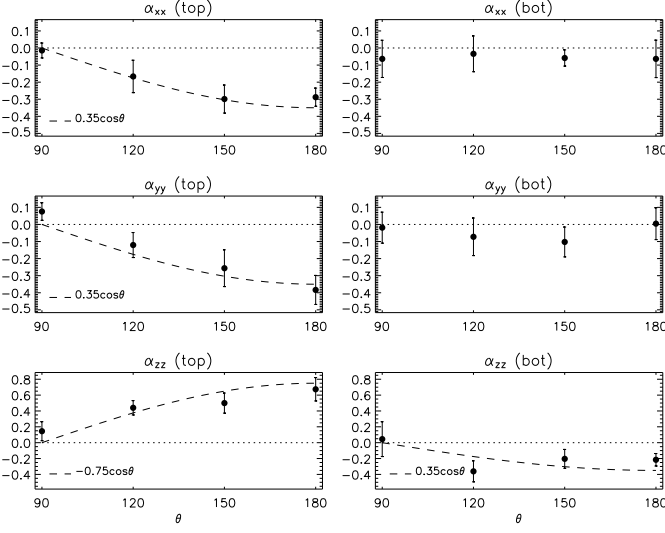


**Fig. 6.** Diagonal components of the  $\alpha$ -tensor for the Co1 set as functions of colatitude in units of  $0.01\sqrt{dg}$  from the top (left panels), and bottom (right panels) of the convectively unstable region (see Fig. 3). The error bars denote conservative error estimates calculated from the full range  $\tilde{\sigma}$ , denoted by the dotted lines in Fig. 3, divided by  $\sqrt{N}$ , where  $N = 10$ . The dashed lines show  $\cos\theta$ -latitude profiles for orientation.

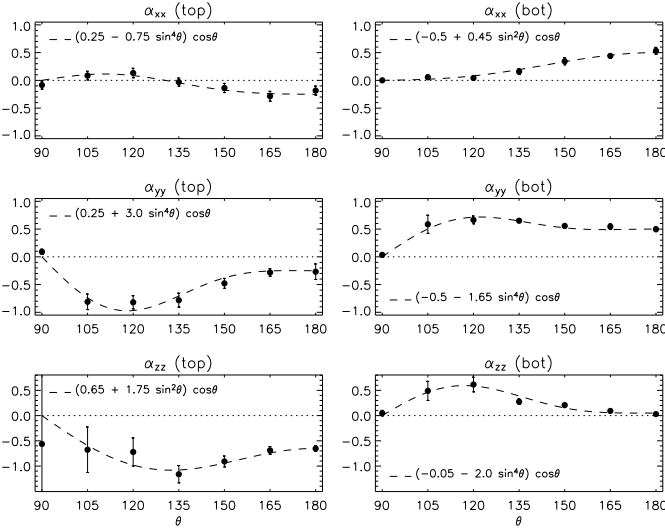


**Fig. 7.** Diagonal components of the  $\alpha$ -tensor for the Co10 set as functions of colatitude in units of  $0.01\sqrt{dg}$  from the top (left panels), and bottom (right panels) of the convectively unstable region (see Fig. 5). The dashed curves show the expressions denoted in the legends of each panel for orientation. Notice the broader plotting range in the panels in the lowermost line. The error bars are computed as in Fig. 6.

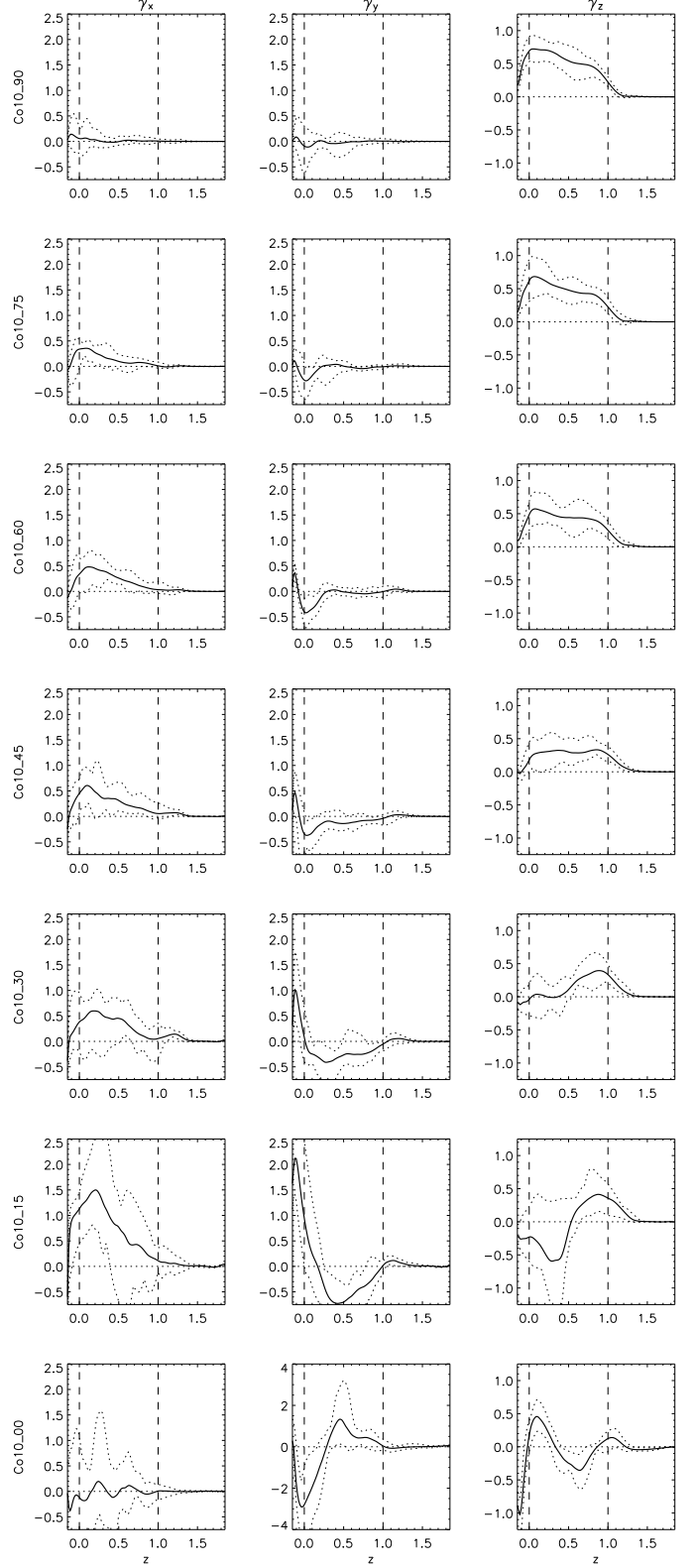


**Fig. 8.** The pumping coefficients according to Eq. (30) from the set Co10 in units of  $0.01\sqrt{dg}$ .

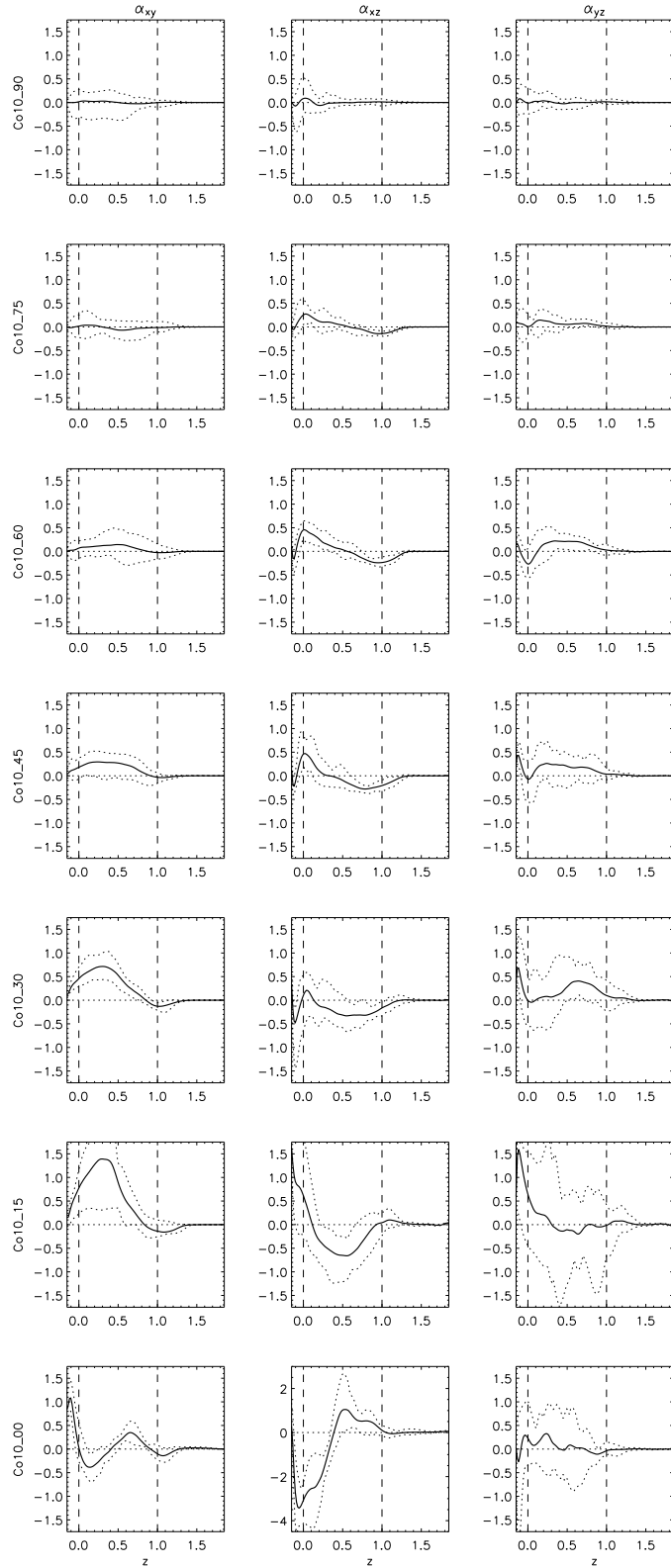


**Fig. 9.** Off-diagonal components of the  $\alpha$ -tensor for the Co10 set in units of  $0.01\sqrt{d/g}$ .

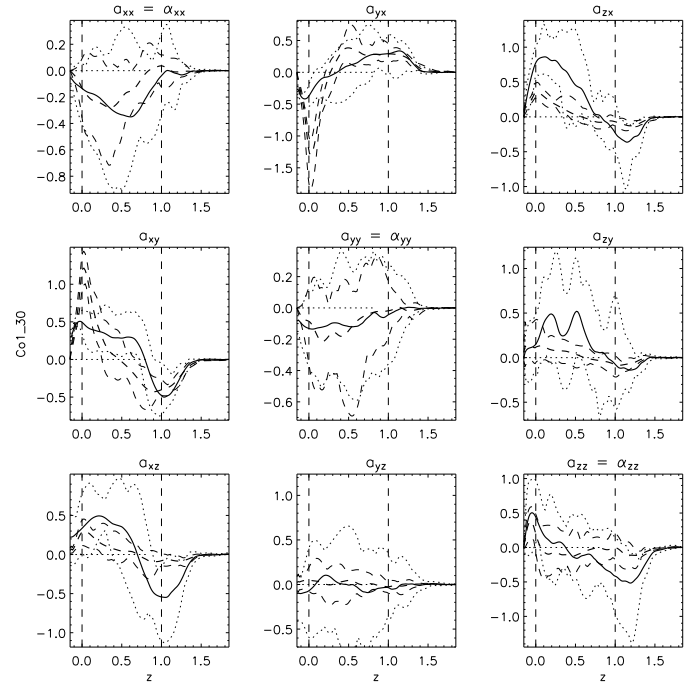


**Fig. 10.** All nine components of the  $a_{ij}$ -tensor for the run Co1-30 (thick solid curves) and the corresponding first order smoothing results (thick dashed curves) according to Eqs. (44) to (52).  $\tau_c = 3\sqrt{d/g}$  in all of the plots. The thin dotted and dashed lines give the full range of values for the full numerical results and the FOSA equivalents, respectively.

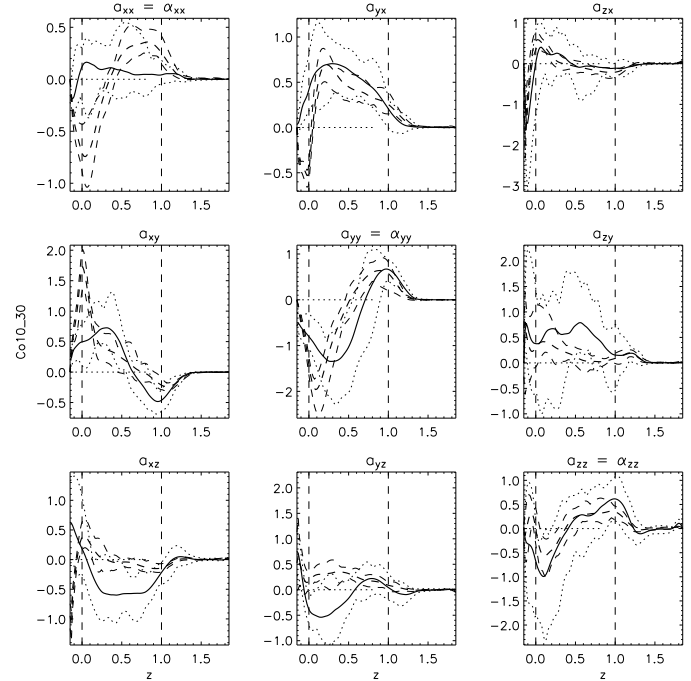


**Fig. 11.** All nine components of the  $a_{ij}$ -tensor for the run Co10-30 (thick solid curves) and the corresponding first order smoothing results (thick dashed curves) according to Eqs. (44) to (52).  $\tau_c = 3\sqrt{d/g}$  in all of the plots. Otherwise the same as Fig. 10.

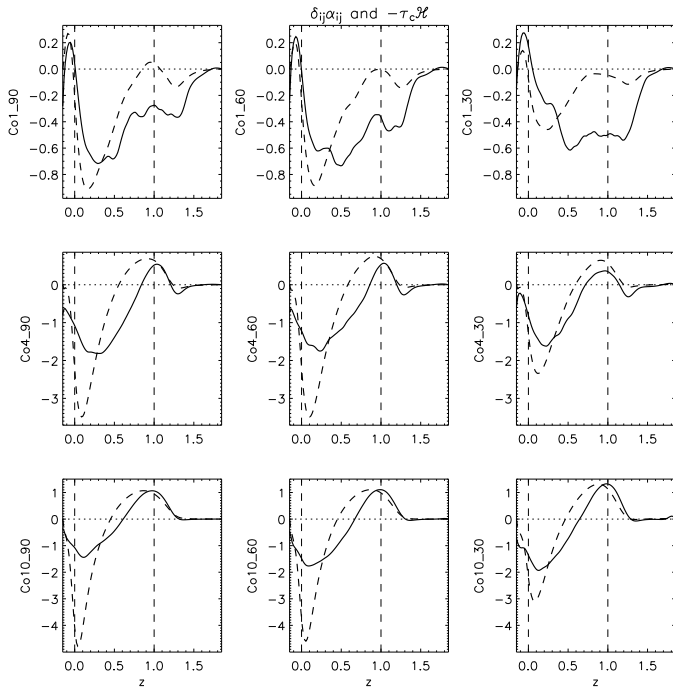


**Fig. 12.** The sum of the diagonal components of  $a_{ij}$  (solid curves), and  $-\tau_c \overline{\boldsymbol{\omega} \cdot \mathbf{u}}$  (dashed curves) as functions of depth. Both quantities are given in units of  $0.01\sqrt{dq}$ . The leftmost column gives data at latitude  $-90^\circ$ , the middle from  $-60^\circ$ , and the rightmost from  $-30^\circ$ . The results at the equator are not shown. The uppermost panel gives results for slow ( $Co = 1$ ), the middle for moderate ( $Co = 4$ ), and the lower for rapid ( $Co = 10$ ) rotation.